

Optical identification of XMM sources in the CFHTLS

C. S. Stalin^{1*}, Patrick Petitjean², R. Srianand³, A. J. Fox⁴, F. Coppolani², A. Schwobe⁵

¹*Indian Institute of Astrophysics, Koramangala, Bangalore 560 034, India*

²*Institut d'Astrophysique de Paris, CNRS - Université Pierre et Marie Curie, 98bis bd Arago, 75014 Paris, France*

³*Inter University Center for Astronomy and Astrophysics, Post Bag 4, Ganesh Khind, Pune 411 007, India*

⁴*European Southern Observatory, Alonso de Córdova 3107, Casilla 19001, Vitacura, Santiago 19, Chile*

⁵*Astrophysikalisches Institut Potsdam, An der Sternwarte 16, D-14482 Potsdam, Germany*

ABSTRACT

We present optical spectroscopic identifications of X-ray sources in ~ 3 square degrees of the XMM-Large Scale Structure survey (XMM-LSS), also covered by the Canada France Hawaii Telescope Legacy Survey (CFHTLS), obtained with the AAOmega instrument at the Anglo Australian Telescope. In a flux limited sample of 829 point like sources in the optical band with $g' \leq 22$ mag and the $0.5 - 2$ keV flux ($f_{0.5-2\text{keV}} > 1 \times 10^{-15}$ erg cm⁻² s⁻¹), we observed 695 objects and obtained reliable spectroscopic identification for 489 sources, $\sim 59\%$ of the overall sample. We therefore increase the number of identifications in this field by a factor close to five. Galactic stellar sources represent about 15% of the total (74/489). About 55% (267/489) are broad-line Active Galactic Nuclei (AGNs) spanning redshifts between 0.15 and 3.87 with a median value of 1.68. The optical-to-X-ray spectral index (α_{ox}) of the broad-line AGNs is 1.47 ± 0.03 , typical of optically-selected Type I quasars and is found to correlate with the rest frame X-ray and optical monochromatic luminosities at 2 keV and 2500 Å respectively. Consistent with previous studies, we find α_{ox} not to be correlated with z . In addition, 32 and 116 X-ray sources are, respectively absorption and emission-line galaxies at $z < 0.76$. From a line ratio diagnostic diagram it is found that in about 50% of these emission line galaxies, the emission lines are powered significantly by the AGN. Thirty of the XMM sources are detected at one or more radio frequencies. In addition, 24 sources have ambiguous identification: in 8 cases, two XMM sources have a single optical source within $6''$ of each of them, whereas, 2 and 14 XMM sources have, respectively, 3 and 2 possible optical sources within $6''$ of each of them. Spectra of multiple possible counterparts were obtained in such ambiguous cases.

Key words: galaxies:active, galaxies:quasars,surveys, X-rays:general

1 INTRODUCTION

Sky surveys play a key role in astronomy as they provide the basic data for the characterization of different populations of astronomical objects and their evolution over cosmic time. We take advantage here of two surveys of the same field: (i) the XMM-Large Scale Structure Survey (XMM-LSS; Pierre et al. 2004) to survey the X-ray sky to a relatively low flux limit of 1×10^{-15} erg s⁻¹ cm⁻² in the $0.5-2$ keV band and (ii) the Wide part of Canada France Hawaii Telescope Legacy Survey (CFHTLS; Cuillandre & Bertin 2006) to observe limited portions of the sky to faint magnitude limits in five optical bands.

The vast majority of the AGNs known today were discovered during optical surveys like the bright Palomar

Quasar Survey (PG; Schmidt & Green 1983), the Large Bright Quasar Survey (LBQS; Hewett et al. 1995), the Hamburg-ESO Quasar Survey (HES; Reimers, Koehler & Wisotzki 1996) the Two Degree Field Quasar Survey (2dF; Croom et al. 2001) and the Sloan Digital Sky Survey (SDSS; Schneider et al. 2007). Such optical colour selection based on wide photometric bands can miss the obscured AGNs. The SDSS survey has identified many type 2 AGNs based on the presence of narrow emission lines in their spectra without broad lines, and with emission line ratios typical of AGN (Kauffmann et al. 2003; Zakamska et al. 2003). Alternatively, X-ray surveys include AGNs without narrow emission lines or those at high redshift where emission line selection is not possible. This is why the identification of X-ray sources down to low optical magnitudes is an important step towards elucidating AGN activity.

There are a number of existing surveys in various en-

* E-mail: stalin@iiap.res.in

ergy bands in the X-ray wavelength range such as the EMSS (Einstein Extended Medium Sensitivity Survey; Maccacaro et al. 1982; Stocke et al. 1991), the ROSAT Bright Survey (Schwope et al. 2000) and the ASCA survey (Ueda et al. 2003), but they all are of relatively poor sensitivity. There are however deep surveys with ROSAT such as the UDS (ROSAT Ultra Deep Survey; Lehmann et al. 2001) and the RDS (ROSAT Deep Survey; Hasinger et al. 1998). They reach an X-ray flux limit of $\sim 10^{-15}$ erg cm $^{-2}$ s $^{-1}$, however over very small regions in the sky. With the *Chandra* and *XMM Newton* X-ray telescopes in operation, X-ray surveys have been significantly boosted. Surveys carried out using XMM-Newton and *Chandra* include the SXDS (Subaru/XMM-Newton Deep Survey; Ueda et al. 2008), LALA (Large Area Lyman Alpha Survey; Wang et al. 2004), CLASXS (Chandra Large Area Synoptic Survey, Yang et al. 2004), ChaMP (Chandra Multiwavelength Project; Kim et al. 2004), CDF-S (Chandra Deep Field-South; Luo et al. 2008; Szokoly et al. 2004), CDF-N (Chandra Deep Field-North; Barger et al. 2003), Bootes Survey (Brand et al. 2006), HELLA2XMM (Cocchia et al. 2007) and the XMM-COSMOS survey (Brusa et al. 2007; Cappelluti et al. 2009; Trump et al. 2009). Most of these X-ray surveys are either deep/ultra-deep pencil beam surveys or shallow large area surveys.

The XMM-LSS survey is a medium depth survey conducted with XMM Newton in the CFHTLS region. It is designed to provide a well defined statistical sample of X-ray selected galaxy clusters out to a redshift of unity, over a large area suitable for cosmological studies (Pierre et al. 2004). Apart from finding new galaxy clusters, XMM-LSS will also provide X-ray point-like sources down to low flux levels, of which AGNs might represent $\sim 95\%$ (Pierre et al. 2007) as they are known to be strong X-ray emitters (Fabbiano et al. 1992) in comparison to normal galaxies. These AGNs are thought to be at the origin of most of the X-ray background (Giacconi et al. 2002; Alexander et al. 2003). Recently, about 80% of the background has been resolved in the 2–10 keV energy range by deep *Chandra* and XMM-Newton observations (e.g. Worsley et al. 2005; Hickox & Markevitch 2006; Carrera et al. 2007). Optical identification of such XMM sources is of great importance to characterize the AGN population as a function of redshift and address specific issues related to the importance of the AGN phenomenon in galaxy formation and evolution of the intergalactic medium. There is an overlap between the XMM-LSS and surveys at different wavelengths: the VIMOS VLT Deep Survey (VVDS; Le Fèvre et al. 2004) and the CFHTLS in the optical, the UKIRT Infrared Deep Sky Survey (UKIDSS; Dye et al. 2006; Lawrence et al. 2007) in the near IR, the *Spitzer* Wide Area InfraRed Extragalactic Legacy Survey (SWIRE; Lonsdale et al. 2003), radio observations from the VLA at 1.4 GHz (Bondi et al. 2003) and at 325 and 74 MHz (Cohen et al. 2003), 610 MHz observations from GMRT (Bondi et al. 2007) and UV observations with GALEX (Arnouts et al. 2005; Schiminovich et al. 2005). In this work, we use version 1 of the XMM-LSS X-ray catalogue (Pierre et al. 2007). Sources were entered in the catalogue if the likelihood of detection in either of the survey bands is greater than 15, and if the observed flux is larger than a 0.5 – 2keV flux limit of 1×10^{-15} erg cm $^{-2}$ s $^{-1}$.

In this paper we present optical spectroscopic identi-

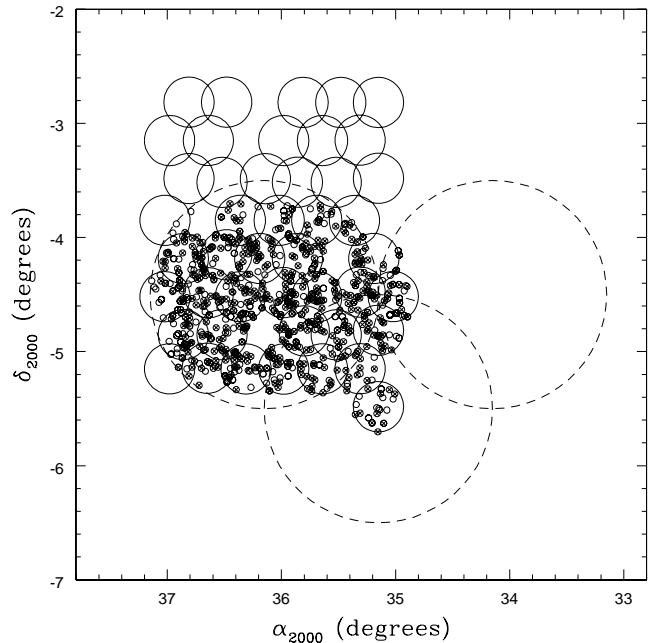


Figure 1. Layout of the 45 XMM-LSS pointings (large closed circles). The positions of our initial sample of 829 sources with $g' < 22$ mag and flux in the 0.5–2 keV band larger than 1×10^{-15} erg cm $^{-2}$ s $^{-1}$ are marked with open small circles. Crosses show the XMM sources for which reliable spectroscopic identifications are obtained in this work. The upper half of the XMM-LSS pointings do not have corresponding optical coverage in CFHTLS. The larger dashed circles are the three AAT pointings

fication of these XMM sources in ~ 3 square degrees of the CFHTLS down to $g < 22$ mag. This spectroscopic campaign is intermediate between large scale but shallower surveys like the 2dF (Croom et al. 2001) or SDSS (Schneider et al. 2007) and deeper but spatially restricted surveys like the VVDS (Gavignaud et al. 2006) which has a limiting magnitude of $I_{AB} < 24$, the AGN survey in the COSMOS field (Trump et al. 2009) reaching a magnitude limit of $i < 23.5$ and optical identification of XMM sources in the ELIAS-S1 field reaching down to $R \sim 24.5$ (Feruglio et al. 2008).

Identifications of X-ray sources in the XMM-LSS have been already obtained by Tajer et al. (2006) and Garcet et al. (2007). The former authors survey sources detected in 1 square degree with $F_{2-10keV} > 10^{-14}$ erg cm $^{-2}$ s $^{-1}$ in the 2–10 keV band at a significance $\geq 3\sigma$ and report 122 unambiguous identifications. The later authors present identification of 99 sources with $R \leq 22$ mag. Here we increase by a factor close to five the number of identifications in this field. The paper is organized as follows. We present the selection of targets in Section 2; Section 3 describes the spectroscopic observations; identifications are discussed in Section 4; Section 5 gives the discussion of results and conclusions are summarized in the final section. Throughout this paper we adopt a cosmology with $H_0 = 70$ km s $^{-1}$ Mpc $^{-1}$, $\Omega_M = 0.27$ and $\Omega_\Lambda = 0.73$.

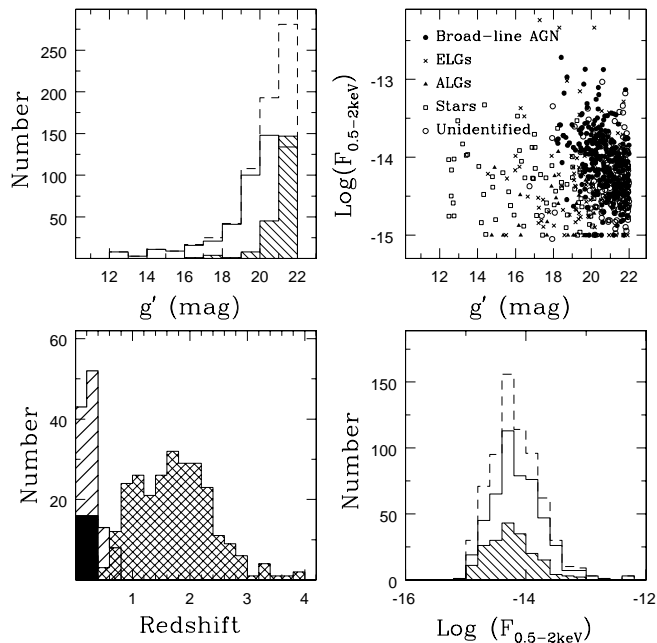


Figure 2. *Top left panel:* g' magnitude distribution of XMM sources observed in this work (dashed histogram), sources with certain identifications (solid histogram) and un-identified sources (hatched histogram). *Bottom left panel:* Redshift distribution of broad-line AGNs (cross hatched region), emission-line objects (hatched region) and absorption-line galaxies (shaded region). *Top right panel:* plot of the X-ray flux at 0.5–2keV ($\text{erg cm}^{-2} \text{s}^{-1}$) band against the optical g' magnitude for broad-line AGNs (filled circles), emission line galaxies (crosses), absorption line galaxies (filled triangles), stars (open squares) and un-identified sources (open circles). *Bottom right panel:* X-ray flux distribution in 0.5–2keV ($\text{erg cm}^{-2} \text{s}^{-1}$) band for our initial sample (dashed histogram), the spectroscopically identified sources (solid histogram) and the un-identified sources (hatched region).

2 OPTICAL AND X-RAY SURVEYS

The basic data sets used to select the targets for this survey are from the XMM-LSS (Pierre et al. 2004) and the wide synoptic component (W1) of CFHTLS.¹

2.1 CFHTLS

The CFHTLS is an ambitious imaging program that has been carried out at the 3.6m Canada-France Hawaii Telescope using the wide field prime focus MegaPrime equipped with MEGACAM, a 36 CCD mosaic camera each of them with 2048×4612 pixels². The pixel scale is $0.185''$, thus giving a total field of view of $0.96 \times 0.94 \text{ deg}^2$. CFHTLS consists of a deep survey in 4 fields (D1, D2, D3 and D4) each covering about 1×1 square degree and a shallower survey on four wide fields (W1, W2, W3, W4) each covering 7×7 square degrees in u^* , g' , r' , i' and z' filters. Final limiting magnitudes in the wide fields should be of the same order in the five bands and typically $i \sim 24.5$. The internal accuracy of the astrometric solution (band to band) is better than one pixel

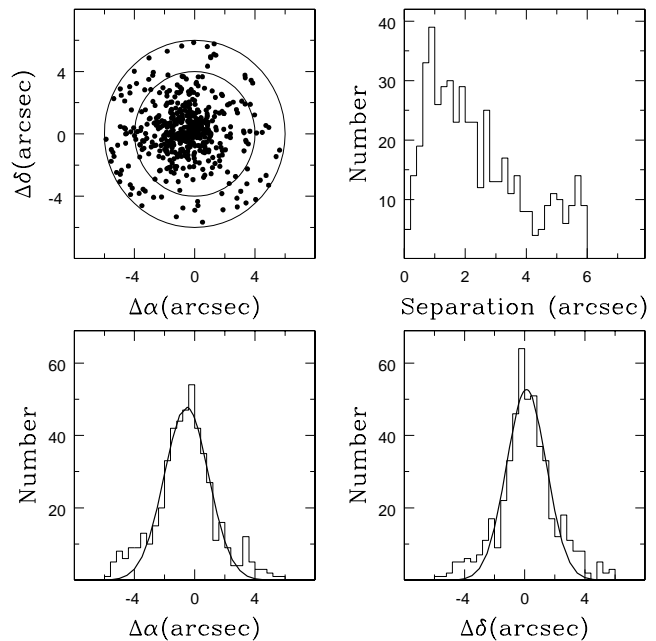


Figure 3. *Top panels:* Offsets between the XMM and optical (XMM – optical) positions (left) and the distribution of the angular separation between the XMM and the optical positions (right) of the spectroscopically identified X-ray sources. Circles in the top left panel have radius of $4''$ and $6''$ respectively. *Bottom panels:* Offset histograms for $\Delta\alpha$ (left) and $\Delta\delta$ (right). The solid line is the gaussian fit to the distribution of offsets. Note the fit is not a good representation of the data and an offset of about $0.15''$ is present in the α direction.

rms over the entire MEGACAM field, whereas the external astrometric solution is around $0.25''$ rms (Schultheiss et al. 2006).

2.2 XMM-LSS

XMM-LSS is a medium depth large area X-ray survey designed to map large scale structures in the Universe (Pierre et al. 2004) and is located around coordinates, $\text{RA} = 2^{\text{h}}$ and $\text{Dec} = -4^{\text{deg}}$ (see Fig. 1). Pierre et al. (2007) present the source list obtained from observations of the first 5.5 square degrees (pertaining to 45 XMM pointings) in the 0.5–2 keV and 2–10 keV bands and above a detection likelihood of 15 in either bands. They also provide the list of optical objects extracted from the CFHTLS catalogue and located within a radius of 6 arcsec around each X-ray source. The layout of the XMM-LSS pointings (big circles) is shown in Fig. 1. We extracted from this catalogue the list of X-ray sources having optical counterparts from CFHTLS brighter than $g' = 22$ mag. We thus arrived at 829 XMM sources having an optical counterpart within $6''$ of the X-ray source and brighter than $g' = 22$ mag. The positions of these sources are marked in Fig. 1 with open small circles. Also marked with crosses on these open small circles are the sources that are reliably identified in the course of this work.

¹ <http://www.cfht.hawaii.edu/Science/CFHTLS/>

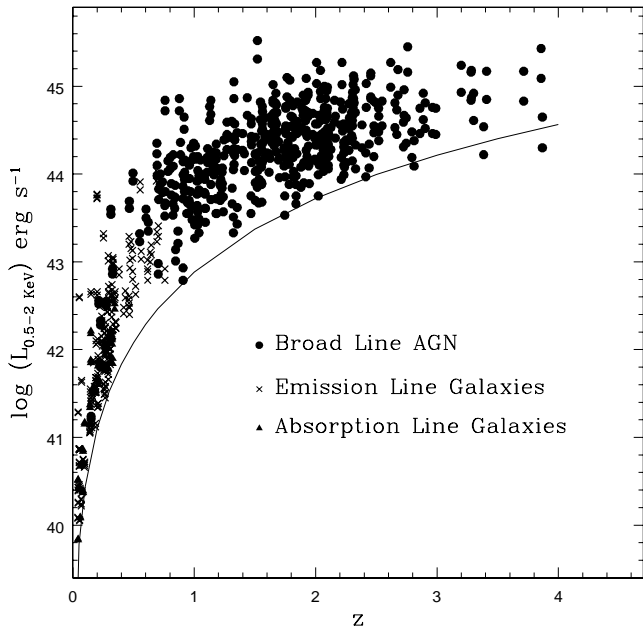


Figure 4. The observed 0.5–2 keV X-ray luminosity of the XMM sources as a function of redshift. Filled circles are for broad-line AGNs, crosses are for emission-line galaxies and filled triangles are for absorption-line galaxies. The line shows the luminosity calculated as a function of redshift for a 0.5–2 keV flux limit of $1 \times 10^{-15} \text{ erg cm}^{-2} \text{ s}^{-1}$.

3 OBSERVATIONS

The spectroscopic observations were performed with the AAOmega system (Sharp et al. 2006) at the 3.9 m Anglo-Australian Telescope (AAT), during the nights of 25, 26, 27 September 2006 and 11, 12, 13 September 2007. AAT observations were focussed on three regions and are shown as three larger circles in Fig. 2. AAOmega involves the multi-object fibre feed from the 2dF fibre positioner system (Lewis et al. 2002) linked to an efficient and stable bench-mounted dual-beam spectrograph. The fibre positioner can place 392 fibres of 2 arcsec projected diameter within a 2 degree field of view. Within each configuration there is a minimum target separation of 30 arcsec imposed by the physical size of the fibre buttons (Miszalski et al. 2006). The dual-beam AAOmega spectrograph, with both blue and red arms, was used in its default low resolution configuration. In the blue arm, the 580V volume phase holographic (VPH) grating was used, providing wavelength coverage between 3700 to 5800 Å sampled at 1 Å/pixel. In the red arm, the 385R VPH grating was used, providing wavelength coverage from 5600 to 8800 Å sampled at 1.6 Å/pixel. The red and blue segments are spliced together between 5600 and 5800 Å thus giving continuous wavelength coverage between 3700 to 8800 Å at a resolution of ~ 1300 . Of the 392 fibres, 25 fibres were assigned to random positions uniformly distributed over the 2 square degrees to sample the background sky and 8 fibre positions were assigned to guide stars within the field. For each plate configuration (each 2 degree field was observed in two to three plate configurations), the observations were broken into blocks of upto 2 hours to minimize flux losses.

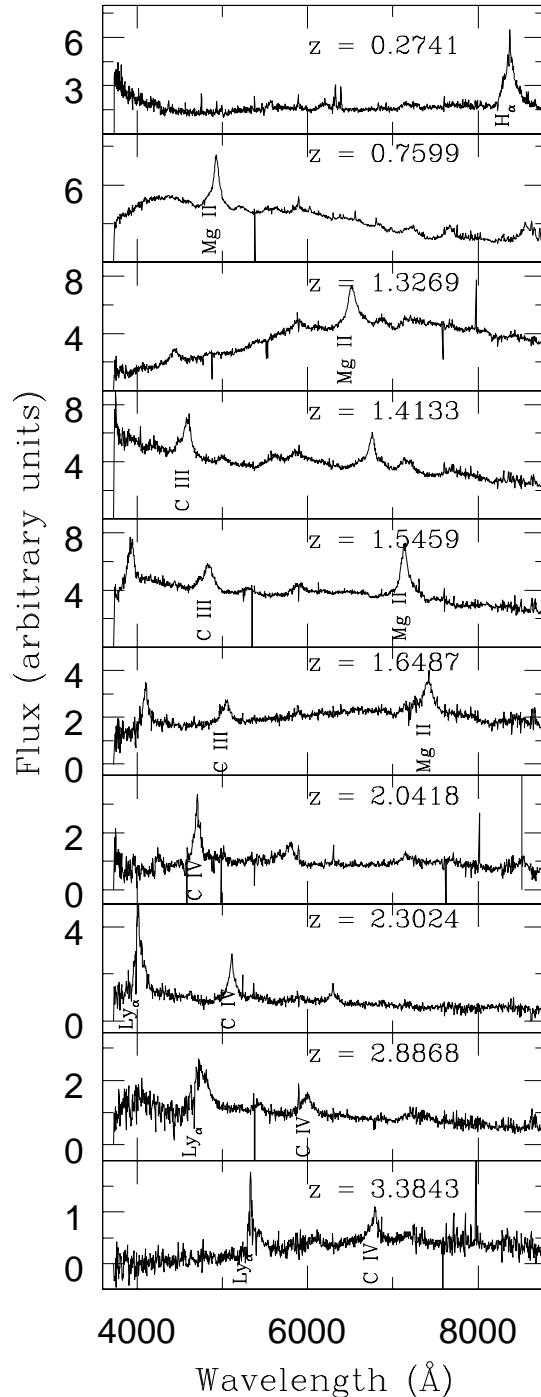


Figure 5. Examples of broad-line AGN optical spectra. In each panels we mark the locations of prominent emission lines and the corresponding redshift of the source.

Each block consists of a quartz-halogen flat field exposure, a composite arc lamp frame for wavelength calibration and three to four science exposures. Total exposure time on each target varies from 10 minutes to 2 hours depending on their brightness. The spectra were not flux calibrated.

Reduction of the observed spectra was performed using

the AAOmega’s data reduction pipeline software DRCONTROL. The two dimensional images were flatfielded, and the spectrum was extracted (using a gaussian profile extraction), wavelength calibrated and combined within DRCONTROL. Redshift estimate was performed using the AUTOZ code (this was kindly provided by Scott Croom). All spectra, identifications and redshift determinations were checked manually. The reduced optical spectra of the 489 identified XMM sources are available upon request.

4 IDENTIFICATION AND CLASSIFICATION OF X-RAY SOURCES

From the initial sample of 829 optical counterparts to XMM sources brighter than $g' = 22$ mag, we were able to obtain spectra for a total of 695 sources. Of these, 489 spectra ($\sim 70\%$) are of sufficient S/N to identify their nature. Standard classification schemes (e.g. Caccianiga et al. 2008) were used to classify these objects from the spectral features detected in their spectra. The g' -band magnitude distribution of our observed sample of 695 sources (dashed histogram), the 489 spectroscopically identified XMM sources (solid histogram) and the 206 unidentified sources (hatched region) are shown in the top left panel of Fig. 2. The bottom left panel of Fig. 2 shows the redshift distributions of broad-line AGNs (cross hatched region), emission line galaxies (sparsely shaded region) and absorption-line galaxies (darkly shaded region). In the top right panel of Fig. 2 is shown the X-ray flux (0.5–2keV) against the optical g' -band magnitude for broad-line AGNs (filled circles), emission line galaxies (crosses), absorption line galaxies (filled triangles), stars (open squares) and unidentified sources (open circles). The bottom right panel of Fig. 2 shows the 0.5–2keV flux distribution of the observed sources (dashed histogram), the spectroscopically identified sources (solid histogram) and the unidentified sources (hatched region) respectively. The distribution of the angular separation between the X-ray and optical positions of the 489 sources is shown in Fig. 3. Also shown in this figure are the histograms of the offsets in α and δ ($\alpha_{XMM} - \alpha_{optical}$; $\delta_{XMM} - \delta_{optical}$) along with a gaussian fit to the distributions. The fitted gaussian function does not reproduce well the real distribution beyond $4''$. 406 sources (83%) are within the $4''$ error circle and their identification is probably secure. It is possible that some of the optical counterparts with larger offsets ($> 4''$) are not correctly identified. The $\Delta\delta$ distribution is found to be symmetrically distributed around zero, whereas the $\Delta\alpha$ distribution is offset by about $0.15''$. This shift in α might be due to systematics in the astrometric corrections applied in the XMM-LSS catalogue (Pierre et al. 2007). The intrinsic X-ray luminosity of these sources plotted against their redshift is shown in Fig. 4 together with the curve marking the position of a source with a 0.5–2 keV flux limit of 1×10^{-15} erg cm^{-2} s^{-1} .

Among the spectroscopically classified 489 sources, we find 267 broad-line AGNs (BLAGNs; $\sim 55\%$ of the identifications), 116 emission-line galaxies (ELGs; $\sim 24\%$ of the sample), 32 absorption-line galaxies (ALGs; $\sim 6\%$ of the sample), and 74 stars ($\sim 15\%$ of the sample). Among the 116 ELGs, based on Baldwin-Phillips-Terlevich (BPT) diagnostic diagram (Baldwin, Phillips, Terlevich 1981), emission lines in 55

Table 1. Statistics of the spectroscopic identifications of XMM sources. Column 1 is the object type, column 2 is the number of unambiguous identifications and column 3 gives the respective percentage.

Object Type	Total Number	Percentage
BLAGN	267	38.4
ELG	116	16.7
ALG	32	4.6
Stars	74	10.6
Unidentified	206	29.7
Total	695	100.0

ELGs are consistent with them being powered significantly by AGN and 61 by starbursts (see below). A summary of these numbers is given in Table 1. Details of these 489 objects are given in Table 2. For most of the sources with spectral lines in our spectroscopic sample, we were able to obtain a reliable estimate of the redshift. This is because for these sources, we were able to identify two or more lines in their spectra. We assign a quality flag (indicative of the reliability of the redshift) $Q = 1$ for those sources. For sources, with only one broad or narrow emission/absorption line in their optical spectra, the redshift estimate is not secure as it is degenerate with more than one possible redshifts. For such sources, we assign a quality flag $Q = 2$. For some sources, the spectral classification is unambiguous, however, the spectra is of poor quality. For these sources, we have assigned a quality flag $Q = 3$. For 206 sources, spectral classification was not possible due to the poor quality of their spectra. Such sources have faint optical magnitudes and this is clearly seen in the top left panel in Fig. 2. In our 489 identified sources, 434, 7 and 48 sources have quality flags Q1, Q2 and Q3 respectively.

4.1 Broad line AGNs

Objects having at least one of the emission lines ($\text{Ly}\alpha$, $\text{CIV}\lambda 1549$, $\text{CIII}\lambda 1909$, $\text{MgII}\lambda 2800$, $\text{H}\beta$ and $\text{H}\alpha$) of width > 2000 km/s are classified as broad-line AGNs. They include Type I Seyferts and quasars. These are sources, in which we are able to have an unobscured view of their central nuclear region (Antonucci 1993). We detect 267 such objects (see Table 1) in our sample corresponding to 55% of the identifications. A few examples are shown in Fig. 5. Redshifts are between $0.15 < z < 3.87$ with a median of $z_{\text{med}} = 1.68$ (see Fig. 2).

We also looked for the presence of Broad Absorption Line (BAL) quasars in our spectroscopic sample. These BAL quasars are characterized by the presence in their spectra of strong absorption troughs blueshifted relative to the QSO emission redshift by 5000 to 50,000 km/s. Seven of the XMM sources we have identified are BALs at $z > 1.5$ based on the presence of strong CIV absorption. Further details on these objects will be reported in a specific paper focussed only on BALs (Stalin et al. 2009a).

Table 2. Properties of the optical identification of the XMM sources. Only the first ten entries are shown. The table in its entirety is available in the electronic edition. Here column 1 is XMM ID, column 2 is optical α , column 3 is optical δ , column 4 is the angular separation between the XMM and optical position, column 5 is g' magnitude, column 6 is redshift, column 7 is the quality flag of the spectra, column 8 is α_{ox} and column 9 is our spectroscopic identification. Objects detected by Spitzer are indicated as SWIRE in the last column

XMM ID	α_{2000} (optical)	δ_{2000} (optical)	sep ($''$)	g' (mag)	z	Q	α_{ox}	ID	Spitzer
XLSS J021934.6-044140	2:19:34.702	-4:41:41.022	1.16	20.84	2.10	1	-1.42	QSO	SWIRE
XLSS J021935.6-042543	2:19:35.932	-4:25:46.048	5.12	20.95	2.48	1	-1.38	QSO	
XLSS J021941.1-044059	2:19:41.160	-4:41:00.311	0.69	20.77	2.10	1	-1.30	QSO	SWIRE
XLSS J021946.9-043754	2:19:47.121	-4:37:54.632	1.89	20.06	1.62	1	-1.56	QSO	SWIRE
XLSS J021951.2-043417	2:19:51.233	-4:34:16.203	0.88	20.84	1.91	1	-1.35	QSO	SWIRE
XLSS J021952.0-040918	2:19:52.149	-4:09:19.867	1.99	20.37	0.69	1	-1.21	QSO	SWIRE
XLSS J021952.3-042447	2:19:52.374	-4:24:48.675	1.84	21.70	0.56	1	-1.34	ELG	
XLSS J021957.2-043952	2:19:57.248	-4:39:52.421	0.59	18.25	2.07	1	-1.67	QSO	SWIRE
XLSS J021958.1-041712	2:19:58.133	-4:17:07.659	4.62	21.12	1.84	3	-1.62	QSO	SWIRE
XLSS J022000.1-041746	2:20:00.159	-4:17:45.391	0.86	21.81	0.92	1	-1.00	QSO	SWIRE

Table 3. Summary of the optical sources having two nearby XMM sources. All optical sources are found to be quasars

XMM-ID	α_{2000} (optical)	δ_{2000} (optical)	Sep ($''$)	z
J022046.1-042032	2:20:46.209	-4:20:38.382	5.72	2.10
J022046.2-042038			1.08	
J022245.5-041928	2:22:45.849	-4:19:32.133	5.06	1.27
J022246.0-041932			3.29	
J022336.8-034500	2:23:37.053	-3:44:59.698	2.81	1.33
J022337.3-034458			4.17	
J022339.0-042005	2:23:39.275	-4:20:05.083	3.94	0.46
J022339.3-042000			5.08	
J022624.5-041959	2:26:24.641	-4:20:02.212	2.84	2.23
J022624.7-042005			3.93	
J022643.5-041629	2:26:43.937	-4:16:27.062	5.77	0.23
J022643.9-041625			1.21	
J022647.1-041038	2:26:47.516	-4:10:37.350	5.57	2.08
J022647.5-041035			2.14	
J022733.9-042224	2:27:34.206	-4:22:28.534	5.69	1.14
J022734.2-042227			1.97	

4.2 Absorption line galaxies (ALGs)

Objects visually identified by the 4000 Å continuum break and absorption features such as CaII-HK $\lambda\lambda$ 3934,3968 and with no obvious presence of emission lines are classified as absorption-line galaxies. We do not impose any limit on the equivalent width of emission lines. Some examples of observed ALGs are shown in Fig. 6. We have identified 32 XMM sources as ALGs. They lie in the redshift range $0.04 < z < 0.34$. The possible nature of this sample of ALGs is further discussed in Section 5.2.

4.3 Emission line galaxies (ELGs)

Sources with narrow emission lines, but with no obvious AGN features in their optical spectra (e.g. high ionization and/or broad lines) are classified as emission-line galaxies (ELGs). Examples of ELG spectra are shown in Fig. 7. Typical emission lines are OII λ 3727, H β , [OIII] λ 4959,5007, H α etc. Other features include CaII-H-K $\lambda\lambda$ 3934,3968 ab-

sorption, the continuum break at ~ 4000 Å, and narrow [NeIII] λ 3869 emission. We have identified 116 ELGs in the redshift range $0.02 < z < 0.76$ (median $z_{\text{med}} = 0.26$).

This classification does not rule out the presence of some underlying AGN activity in ELGs. The dominant energy source (AGN or starburst), can be identified using the commonly used BPT diagnostic diagrams (Baldwin, Phillips, Terlevich 1982). The ratios of nebular emission lines ([OIII] λ 5007/H β) and ([NII] λ 6593/H α) are used to distinguish the ionising source i.e., between thermal continuum from starbursts and non-thermal AGN continuum. The BPT diagram for our sample of ELGs is shown in Fig. 8 together with the two empirical relations commonly used to classify the emission-line objects into AGNs (points above the curves) or starbursts (below the curves):

$$\log([OIII]/H\beta) = \frac{0.61}{[\log([NII]/H\alpha) - 0.05]} + 1.3 \quad (1)$$

$$\log([OIII]/H\beta) = \frac{0.61}{[\log([NII]/H\alpha) - 0.47]} + 1.19 \quad (2)$$

Eq. 1 is given by Kauffmann et al. (2003) and Eq. 2 by Kewley et al. (2001). However, there are sources for which we are not able to measure both the [NII]/H α or the [OIII]/H β line ratio. In such cases, an ELG is thought to be powered by an AGN if it has $\log([NII]/H\alpha) > -0.2$ or $\log([OIII]/H\beta) > 0.9$ and by a starburst otherwise if we take Kauffmann et al. (2003) relation. On the other hand, if we consider Kewley et al. (2001) relation an ELG is thought to be powered by an AGN if it has $\log([NII]/H\alpha) > 0.3$ or $\log([OIII]/H\beta) > 1.0$. Based on the above line ratio diagnostics and following Kauffmann et al. (2003), of the 116 emission-line galaxies, 61 are powered significantly by starbursts and the remaining 55 are significantly powered by AGN (so about 50%). Alternately if we consider Kewley et al. (2001) relation, in the sample of 116 ELGs, 82 are powered by starbursts and 31 are powered by AGN. Another criteria to separate the ELGs with X-ray emission dominated by stellar processes rather than AGN activity is to look into their X-ray to optical flux ratio (f_x/f_o ; Fiore et al. 2003 (see Figure 5)). If $f_x/f_o < 0.01$ it is a normal star-

forming galaxy and if $f_x/f_o > 0.1$ it is an AGN (Kim et al. 2006). We define $\log(f_x/f_o)$ as

$$\log(f_x/f_o) = \log(f_x) + 5.41 + \frac{g'}{2.5} \quad (3)$$

Here f_x is the flux in the 0.5–2keV band and g' is the optical magnitude. The constant comes from the conversion of AB g' magnitude into monochromatic flux and integration of the monochromatic flux over the g' bandwidth assuming a flat spectrum. Fig. 9 shows f_x/f_o versus the intrinsic X-ray luminosity in the 0.5–2 keV band, $\log(L_{(0.5-2keV)})$ for the broad-line AGNs, the two classes of ELGs found from the BPT diagram (those significantly powered by AGN and starburst) and ALGs. From the figure it is clear that the broad-line AGNs in our spectroscopic sample occupy a distinct location in the $\log(f_x/f_o)$ v/s $\log(L_{(0.5-2keV)})$ plane. ELGs and ALGs of our sample mostly occupy the region with intrinsic X-ray luminosity $L_{0.5-2keV} < 10^{43}$ erg s^{-1} . It thus seems that at $L_{0.5-2keV} < 10^{43}$ erg s^{-1} the ELGs population in our sample is made of a mixture of normal star-forming galaxies, low-luminosity AGNs and galaxies powered by starbursts with high star-formation rates. In all further discussions, we however, use the Kauffmann et al. (2003) relation to separate ELGs powered predominantly by AGN and starburst respectively.

4.4 Stars

As in other deep X-ray surveys, our sample also contains about 15% (74 objects) of galactic stars as optical counterparts to XMM sources (at $z = 0$). They are typically G, K and M-type stars whose X-ray emission is caused by magnetic activity (Brandt & Hasinger 2005). A few spectra are shown in Fig. 10.

4.5 Multiple optical counterparts

In our spectroscopic sample, there are 8 cases for which two XMM sources have the same optical counterpart within 6 arcsecs of each of the XMM sources. The details of these 8 sources are given in Table 3. In all these cases the optical counterpart is a quasar. We find also 16 XMM sources having more than one optical counterpart within 6 arcsecs of them. Spectra of all possible counterparts of the 16 XMM sources were obtained and all are classified based on their spectral appearance. The details of these sources are shown in Table 4. Of these, the two XMM sources, XLSS J022600.1–035955 and XLSS J022630.7–050550, are associated with a quasar-galaxy pair. It is more than probable that the XMM source counterpart is the quasar. Note that XLSS J022536.4–050011 is also associated with a radio source in the NVSS with a 1.4 GHz flux density of 12 mJy (see Table 5).

4.6 Multiwavelength counterparts

4.6.1 Correlation with radio surveys

We cross-correlated the 489 newly identified XMM sources with the publicly available National Radio Astronomical Observatory VLA sky survey (NVSS; Condon et al 1998) at 1.4 GHz. Only 21 XMM sources are detected in NVSS.

We also cross-correlated our 489 identified sources with low frequency radio observations performed in this field with GMRT at 240 and 610 MHz (Tasse et al. 2007). There are 12 objects detected at 240 MHz, while another 22 objects are detected at 610 MHz. In total 34 objects are detected in one of the radio bands. The details of the XMM sources with radio detections are given in Table 5.

4.6.2 Correlations with IR surveys

There is some overlap between the XMM-LSS field and one of the fields observed by the *Spitzer* Wide-area Infrared Extragalactic Survey (SWIRE; Lonsdale et al. 2003). In SWIRE, observations were performed with the Infrared Array Camera (IRAC) at 3.6, 4.5, 5.8 and 80 μ m and with the Multiband Imaging Photometer (MIPS) at 24, 70 and 160 μ m to a 5σ depth of 4.3, 8.3, 58.4, 65.7 μ Jy and 0.24, 15 and 90 mJy respectively (Tajer et al. 2007). Correlating our sample of optically identified XMM sources (489 in total) with SWIRE, we find that $\sim 50\%$ (239 sources) are detected in SWIRE. Of these, 133 are broad-line AGNs, 36 are stars, 50 and 20 are emission and absorption-line galaxies respectively. The positions of these X-ray sources in the IR colour–colour diagram (3.6–4.5 v/s 5.8–8.0 μ m) is shown in Fig. 11. Optical identification and description of SWIRE sources over a larger area in CFHTLS, will be reported in Stalin et al. (2009b).

5 DISCUSSION

5.1 Optical-to-X-ray slope (α_{ox})

The broad band spectral index α_{ox} of any source characterizes the UV to X-ray spectral energy distribution by assuming that the rest frame flux emitted at 2500 \AA can be connected to the one at 2 keV with a simple power law. This is a simple measurement of the amount of X-ray radiation emitted mostly by non-thermal processes with respect to the amount of UV radiation emitted mostly by thermal processes (Kelly et al. 2007). We estimated α_{ox} for each of the spectroscopically identified broad-line AGNs and ELGs (as some of the ELGs are powered by AGN) in our sample. For this we have converted the observed i' -band magnitudes to fluxes following the definition of the AB system (Oke & Gunn 1983)

$$S_{i'} = 10^{-0.4(m_{i'} + 48.60)}. \quad (4)$$

where $S_{i'}$ and $m_{i'}$ are respectively the flux and magnitude in the i' -band. The luminosity at the frequency corresponding to 2500 \AA in the rest-frame is calculated following Stern et al. (2000)

$$L_{\nu_1} = \frac{4\pi D_l^2}{(1+z)^{1+\alpha_o}} \left(\frac{\nu_1}{\nu_2}\right)^{\alpha_o} S_{\nu_2} \quad (5)$$

where ν_2 is the observed frequency corresponding to the i' -band, S_{ν_2} is the observed flux in i' -band, ν_1 is the rest-frame frequency corresponding to 2500 \AA and D_l is the luminosity distance. An optical spectral index $\alpha_o = -0.5$ (Anderson et al. 2007) is assumed ($S_\nu \propto \nu^\alpha$). The luminosity at rest frame 2 keV is obtained using a similar equation

as Eq. 5, assuming a X-ray spectral index of $\alpha_x = -1.5$ (Anderson et al. 2007).

Thus, the broad band spectral index α_{ox} is obtained as

$$\alpha_{\text{ox}} = \frac{\log(L_X/L_{\text{opt}})}{\log(\nu_X/\nu_{\text{opt}})} \quad (6)$$

Here L_X and L_{opt} are the rest frame monochromatic luminosities at 2 keV and 2500Å (erg s⁻¹ Hz⁻¹) respectively. The distribution of α_{ox} (not corrected for intrinsic and galactic absorption) for the sample of spectroscopically identified broad-line AGNs is shown in Fig. 12. A mean value of $\alpha_{\text{ox}} = -1.47 \pm 0.03$ is found for broad-line AGNs which is consistent with the values found in the literature (Strateva et al. 2005).

5.1.1 X-ray luminosity (L_X) versus optical luminosity (L_{opt})

Previous studies of optically-selected quasars have found a strong correlation between the optical and X-ray monochromatic luminosities (Anderson et al. 2007 and references therein). The relation between both luminosities is of the form $L_X \propto L_{\text{opt}}^\beta$. Different values have been derived for β varying typically from 0.7 (Pickering et al. 1994; Wilkes et al. 1994) to 0.8 (Avni & Tananbaum 1986) and up to unity or slightly larger (La Franca et al. 1995; Green et al. 2009). The plot giving the rest frame monochromatic luminosity at 2 keV versus the rest frame optical luminosity at 2500 Å of all the optically identified X-ray sources is shown in Fig. 13 (top panel). It is apparent that a strong correlation exists for broad-line AGNs. Part of the scatter in the X-ray to optical relation in Fig. 13 (top panel) might be related to the variability of the AGNs as the X-ray and optical observations are far from being simultaneous, but we do not expect this effect to be very important. The fit for only the broad-line AGNs gives

$$\log L_X = (0.870 \pm 0.001) \log L_{\text{opt}} + 0.009 \pm 0.370 \quad (7)$$

with a linear correlation coefficient $r = 0.98$. This is slightly lower than the slope of 1.12 found by Green et al. (2009), however, within the range of values found by Steffen et al. (2006) through different regression methods. Note that to perform the fit we excluded radio loud AGNs that can have additional UV and X-ray flux associated with the radio jet (Worrall et al. 1987; Worrall & Birkinshaw 2006; Wilkes & Elvis 1987). Also, radio-loud AGNs are found to be 2–3 times brighter in X-ray for the same optical magnitude (Shen et al. 2006; Zamorani et al. 1981). Therefore we have used only the sample of broad-line AGNs, excluding the 9 AGNs which are found to be detected in the radio (see Table. 5).

5.1.2 α_{ox} versus optical luminosity (L_{opt})

The existence of a correlation between L_X and L_{opt} in broad-line AGNs, in turn implies that α_{ox} correlates also with the X-ray and UV monochromatic luminosities at 2 keV and 2500 Å respectively. Fig. 13(bottom panel) shows the trend of α_{ox} with the rest-frame monochromatic luminosity for our spectroscopic sample. For broad-line AGNs, from a linear least squares fit we found

$$\alpha_{\text{ox}} = (-0.065 \pm 0.019) \log(L_{\text{opt}}) + (0.509 \pm 0.560) \quad (8)$$

This is similar to the value of 0.060 ± 0.007 found by Green et al. (2009) however, flatter than the value of 0.137 ± 0.008 found by Steffen et al. (2006). We do not find any significant correlation between α_{ox} and (L_{opt}) for our sample of ELGs.

5.1.3 Evolution of α_{ox}

The plot of α_{ox} versus redshift is shown in Fig. 14(top panel). The fit to the data in our sample of broad-line AGNs with $\alpha_{\text{ox}} = Az + B$ gives $A = -0.021 \pm 0.015$ and a linear correlation coefficient of 0.07. It thus seems that for broad-line AGNs, α_{ox} does not depend strongly on redshift. This is consistent with the claims of non-evolution already published in the literature (Just et al. 2007; Steffen et al. 2006; Vignali et al. 2003; Strateva et al. 2005; Avni & Tananbaum 1986; Green et al. 2009; however see Yuan et al. 1998; Bechtold et al. 2003). We also tried to check for the evolution of α_{ox} for broad-line AGNs after removal of its luminosity dependence. For this we subtracted the α_{ox} obtained through the best fit $\alpha_{\text{ox}} - L_{\text{opt}}$ regression (Eq. 8) from the observed α_{ox} . We find that this resultant $\Delta\alpha_{\text{ox}}$ for broad line AGNs shows no trend with redshift (Fig. 14 bottom panel). It can be seen in Fig. 14 that for $z < 0.5$, (i) most of the α_{ox} measurements are smaller than -1.6 and (ii) the scatter in the values of α_{ox} is much larger than for higher redshifts. The main reason for this is that the low redshift sources are mostly ELGs (50% of them being significantly powered by AGN). The optical spectrum of these objects firstly is significantly/predominantly contaminated by star-light from the host galaxy and secondly, the derivation of α_{ox} using the optical and X-ray spectral index of AGNs might not be appropriate in ELGs.

An ideal sample to look for the correlations between L_X and L_{opt} , and α_{ox} with either L_X , L_{opt} or z is the one that fills the $L - z$ plane. However, in practice it is difficult and most of the samples in literature used for such correlation searches were based on objects that covers only a narrow range in the $L - z$ plane. Such a sample is also likely to be contaminated with sources with unrelated physical processes such as BALs and radio-loud AGN (Green et al. 2009). We wish to point out that the linear least squares regression analysis presented here is a simple minded approach compared to the detailed statistical analysis performed by Green et al. (2009) that includes upper limits. However as discussed in earlier sections, our results are broadly in line with those available in literature.

5.2 The absorption-line galaxies

The existence of an intriguing population of galaxies with strong X-ray emission ($41 < \log L_X < 44$ erg s⁻¹ in the rest frame energy range 2–8 keV; Rigby et al. 2006) was first noted from observations with the Einstein Observatory (Elvis et al. 1981). The X-ray emission reveals the presence of an AGN without other sign of activity (no emission line is seen in their optical spectrum). Further observations with ROSAT, *Chandra* and *XMM-Newton* have supported the existence of this population (Fiore et al. 2003; Caccianiga et al. 2007; Griffiths et al. 1995; Garcet et al. 2007). Such galaxies are now referred to as X-ray Bright Optically Normal Galaxies (XBONGs).

Table 4. Summary of XMM sources having more than one optical counterpart

XMM– ID	α_{2000} (optical)	δ_{2000} (optical)	Sep. ($''$)	g' (mag)	ID	z
XLSS J022049.4-043030	02:20:49.545	-04:30:28.774	1.77	21.99	QSO	1.04
	02:20:49.501	-04:30:31.265	1.27	21.47	QSO	1.81
XLSS J022105.4-044101	02:21:05.601	-04:41:01.490	1.80	18.31	ELG	0.20
	02:21:05.508	-04:41:03.581	1.63	20.16	ELG	0.20
XLSS J022124.2-042517	02:21:24.264	-04:25:20.231	2.75	19.28	STAR	0.00
	02:21:24.492	-04:25:17.663	3.83	20.25	ELG	0.29
XLSS J022127.7-043407	02:21:27.978	-04:34:10.234	4.38	17.20	ALG	0.21
	02:21:27.567	-04:34:03.263	5.01	20.06	ELG	0.09
XLSS J022159.6-045738	02:21:59.985	-04:57:36.175	5.61	18.45	ELG	0.16
	02:21:59.581	-04:57:38.803	1.08	21.46	ELG	0.16
XLSS J022249.7-044539	02:22:49.768	-04:45:36.907	2.11	19.95	ELG	0.26
	02:22:49.835	-04:45:39.856	1.38	20.52	ELG	0.26
XLSS J022316.0-040503	02:23:16.233	-04:05:08.573	5.75	18.74	STAR	0.00
	02:23:16.091	-04:05:03.988	0.97	21.56	QSO	2.02
XLSS J022329.1-045453	02:23:28.996	-04:54:54.474	3.16	21.40	ELG	0.33
	02:23:29.253	-04:54:51.875	1.59	20.43	QSO	0.60
XLSS J022416.8-050325	02:24:16.997	-05:03:24.466	2.56	18.27	ALG	0.14
	02:24:16.863	-05:03:24.993	0.64	19.21	ALG	0.14
XLSS J022424.8-052037	02:24:24.896	-05:20:36.892	0.73	19.64	ELG	0.28
	02:24:24.984	-05:20:40.063	3.25	21.71	ELG	0.28
XLSS J022536.4-050011	02:25:36.438	-05:00:11.922	1.00	16.00	ELG	0.05
	02:25:36.774	-05:00:07.898	5.43	17.90	ELG	0.05
	02:25:36.289	-05:00:07.697	4.80	18.96	ELG	0.05
XLSS J022558.7-051245	02:25:59.150	-05:12:45.378	5.92	19.35	ELG	0.26
	02:25:59.036	-05:12:47.268	4.49	21.94	ELG	0.26
XLSS J022600.1-035955	02:25:59.881	-03:59:59.003	5.06	18.28	ELG	0.14
	02:26:00.266	-03:59:52.683	3.60	17.32	STAR	0.00
	02:26:00.017	-03:59:54.375	2.29	21.07	QSO	1.09
XLSS J022630.7-050550	02:26:30.742	-05:05:44.427	5.70	20.26	ELG	0.19
	02:26:30.777	-05:05:52.004	1.90	19.86	QSO	1.66
XLSS J022635.1-050518	02:26:35.031	-05:05:20.535	3.09	16.87	STAR	0.00
	02:26:35.259	-05:05:17.719	1.58	17.03	STAR	0.00
XLSS J022647.7-041426	02:26:47.693	-04:14:30.763	4.44	20.78	QSO	2.33
	02:26:47.848	-04:14:26.229	1.48	21.05	ELG	0.26

Their exact nature is unknown although several hypothesis have been advocated in the literature to explain their properties. It has been argued that heavy obscuration by Compton-thick gas covering the nuclear source could prevent ionizing photons from escaping. In this hypothesis, the obscuration must occur in all directions, and should not be restricted to the torus, because the sources lack both broad and narrow lines in their spectra. This idea might be correct for at least some XBONGs (Spoon et al. 2001). Dilution of nuclear emission from the host galaxy starlight could play a role (Georgantopoulos & Gerogakakis 2005). Such an effect might be important if the ground based spectroscopic observations are performed with relatively wide slits. Severgnini et al. (2003) have shown on three objects of their sample, that adequate observations (narrow slit, accurate positioning of the slit etc.) reveal the missing emission lines. They argue that survey observations are sometimes inadequate to completely unveil the true nature of the X-ray sources. However, the intrinsic optical continuum emission of XBONGs is weak compared to that of quasars (Comastri et al. 2002) suggesting that the emission line luminosities are also intrinsically small. XBONGs could be extreme BL Lacs in which the featureless non-thermal continuum is much weaker than the host galaxy starlight. Indeed, there is

one case of a XBONG being associated with a BL Lac object (Brusa et al. 2003) and it has been argued by Fosatti et al. (1998) that XBONGs could belong to the low-luminosity tail of the blazar sequence. However, large calcium break and radio quietness in several XBONGs argue against them being BL Lacs (Fiore et al. 2000). Finally, XBONGs might be powered by an inner Radiatively Inefficient Accretion Flow (RIAF) plus an outer radiatively efficient thin accretion disk (Yuan & Narayan 2004).

In our sample we detect 32 X-ray sources having only absorption lines and devoid of any emission lines. This represent $\sim 6\%$ of our sample of observed sources. They have redshifts ranging between 0.04 and 0.34. These galaxies are located in the peculiar regions of the IR-color-color diagram (see Fig. 11) well outside the AGN location and have also a distinct location in the $L_{opt} - L_X$ plane (see Fig. 13). We further analysed the optical spectra of these sources to see if they could be BL Lacs by looking at the shape of the continuum around the Ca H&K break at 4000 Å. The detection of a significant reduction of the Ca H&K break when compared to normal elliptical galaxies can be considered as an indication of the presence of a substantial non-thermal nuclear continuum emission. To identify the shape of the continuum

Table 5. Summary of XMM sources with radio detections

XMM-ID	α_{2000} optical	δ_{2000} optical	Sep (arcsec)	g' (mag)	z	ID	S_{240MHz} (mJy)	S_{610MHz} (mJy)	$S_{1420MHz}$ (mJy)
XLSS J022001.6-052217	02:20:01.624	-05:22:16.904	0.70	20.12	2.22	QSO	9.6	15.4	15.4
XLSS J022108.2-042759	02:21:08.366	-04:28:01.924	3.05	20.18	0.27	ELG	—	—	2.1
XLSS J022120.1-040217	02:21:20.477	-04:02:17.911	4.54	20.31	0.32	ALG	—	—	3.3
XLSS J022127.7-043407	02:21:27.978	-04:34:10.234	4.38	17.20	0.21	ALG	17.5	11.1	8.3
XLSS J022127.7-043407	02:21:27.567	-04:34:03.263	5.01	20.06	0.09	ELG	17.5	11.1	8.3
XLSS J022144.9-035745	02:21:44.947	-03:57:45.388	0.61	21.45	2.50	QSO	51.6	20.4	9.6
XLSS J022247.7-043330	02:22:47.874	-04:33:30.031	1.42	20.32	1.63	QSO	—	2.4	4.5
XLSS J022251.6-050714	02:22:51.748	-05:07:12.422	2.40	21.53	3.86	QSO	—	—	3.5
XLSS J022255.5-051817	02:22:55.739	-05:18:17.404	3.59	20.85	1.76	QSO	670.2	436.9	259.5
XLSS J022257.9-041840	02:22:57.965	-04:18:40.643	0.37	19.05	0.24	ELG	—	2.8	—
XLSS J022258.4-040709	02:22:58.568	-04:07:15.079	5.62	19.96	0.29	ALG	7.0	—	—
XLSS J022310.2-042304	02:23:10.029	-04:23:04.034	3.63	21.03	0.24	ELG	39.3	52.0	37.2
XLSS J022337.4-040937	02:23:37.439	-04:09:38.303	0.60	14.78	0.00	STA	—	6.6	4.0
XLSS J022345.3-043406	02:23:45.337	-04:34:07.965	1.43	14.94	0.00	STA	—	2.9	3.5
XLSS J022402.4-044135	02:24:02.640	-04:41:34.703	2.25	14.54	0.04	ELG	—	—	4.7
XLSS J022403.7-043303	02:24:03.782	-04:33:04.893	1.49	15.55	0.04	ELG	11.4	6.8	4.0
XLSS J022447.0-040849	02:24:47.000	-04:08:51.096	1.54	17.77	0.10	ELG	—	1.8	—
XLSS J022509.7-050950	02:25:09.712	-05:09:49.145	1.48	20.20	0.32	ALG	—	2.4	—
XLSS J022528.3-041536	02:25:28.348	-04:15:39.796	3.68	21.42	0.56	ELG	—	—	2.4
XLSS J022536.4-050011	02:25:36.438	-05:00:11.922	1.00	16.00	0.05	ELG	33.2	16.3	12.0
XLSS J022536.4-050011	02:25:36.774	-05:00:07.898	5.43	17.90	0.05	ELG	33.2	16.3	12.0
XLSS J022536.4-050011	02:25:36.289	-05:00:07.697	4.80	18.96	0.05	ELG	33.2	16.3	12.0
XLSS J022549.4-040028	02:25:49.766	-04:00:24.460	5.79	16.27	0.04	ELG	—	2.9	—
XLSS J022556.1-044724	02:25:56.092	-04:47:24.403	0.84	21.43	1.01	QSO	—	2.3	2.4
XLSS J022558.7-050055	02:25:58.853	-05:00:54.245	2.24	18.58	0.15	ELG	7.8	6.9	3.2
XLSS J022604.3-045929	02:26:04.510	-04:59:33.441	4.83	16.21	0.05	ELG	—	3.3	—
XLSS J022609.9-045805	02:26:09.666	-04:58:05.615	3.68	15.35	0.05	ALG	—	2.1	—
XLSS J022617.6-050443	02:26:17.408	-05:04:43.312	3.47	15.50	0.05	ELG	20.6	13.1	8.4
XLSS J022618.9-040016	02:26:19.060	-04:00:14.727	2.47	19.85	0.21	ALG	118.8	87.8	—
XLSS J022659.2-043529	02:26:58.959	-04:35:26.615	5.29	14.74	0.07	ALG	—	—	3.2
XLSS J022720.7-044537	02:27:20.692	-04:45:37.166	0.89	15.98	0.05	ELG	6.7	3.2	—
XLSS J022740.5-040250	02:27:40.545	-04:02:50.990	0.72	18.18	2.62	QSO	—	3.3	3.3
XLSS J022758.1-040753	02:27:57.999	-04:07:51.950	2.16	19.43	0.21	ELG	—	—	2.6

around 4000 Å we define D_n (relative flux depression across the Ca H&K break) as

$$D_n = \frac{F^+ - F^-}{F^+} \quad (9)$$

Here F^+ and F^- are the average fluxes in the region 4050–4250 Å and 3750–3950 Å respectively in the source rest frame (Caccianiga et al. 2007). We adopt a limit of $D_n < 40\%$ for a source with no emission line to be a BL Lac object (Caccianiga et al. 2007). Of the 32 sources in our sample 17 have $D_n < 40\%$ and hence could be BL Lac candidates. To further investigate the possibility for these 17 sources to be BL Lac candidates we looked for any sign of radio emission from these objects (this is another indication of the presence of non-thermal emission) both in the literature and the NVSS. Three among the 17 sources with $D_n < 40\%$ are found to be radio emitters. It is thus likely that these 3 objects (XLSS J022509.7–050950, XLSS J022609.9–045805, XLSS J022659.2–043529) are BL Lacs. It is also probable that emission lines in ALGs are weak and could be revealed by deeper observations. It would be interesting to conduct follow-up observations of our sample of 32 absorption-line galaxies to study this population in more detail.

6 CONCLUSIONS

We have presented the optical spectroscopic classification of 489 X-ray sources. They were drawn from an initial sample of 829 X-ray sources detected in the course of the XMM-LSS survey that overlap one of the wide fields of the CFHTLS. The sources have a detection threshold of 15 in either the 0.5–2 keV or 2–10 keV bands and are brighter than 22 mag in the optical g' -band. This sample of 829 X-ray sources is thus flux limited in both X-ray and optical bands. We observed 695 of these objects with the AAOmega system at the AAT of which spectroscopic identification was possible for 489 sources (our sample is therefore ~70% complete). A large fraction of these X-ray sources were identified as BLAGNs (~55%) based on the FWHM of the emission lines present in their spectra. In addition to these BLAGNs, 74 sources are identified as galactic stars, 32 are absorption-line galaxies, and 116 are emission-line galaxies. Based on BPT diagram we find that the emission lines in 55 (61) of the 116 emission line galaxies are powered significantly by an AGN (starburst). For the broad-line AGNs, α_{ox} is found to correlate well with the rest frame monochromatic luminosity at 2500 Å (see also Krumpe et al. 2007, Just et al. 2007, Gibson, Brandt & Schneider 2008, Green et al. 2009). The rest frame X-ray and UV monochromatic luminosities

at 2 keV and 2500 Å respectively are found to be closely correlated for broad line AGNs. No dependence of α_{ox} with redshift is found. This is similar to the results by Just et al. (2007) and Green et al. (2009) but in contrast to Yuan et al. (1998) and Bechtold et al. (2003) studies who found a correlation of α_{ox} with redshift. We detect 32 X-ray emitting galaxies with no sign of AGN activity in their optical spectra. They are found to be located in a well defined part of the IR-color-color diagram. It would be very interesting to perform more focussed observations to investigate the true nature of what seems to be a particular population of X-ray sources.

ACKNOWLEDGMENTS

We thank the anonymous referee for his/her critical comments that led to significant improvement of the paper. We also thank the present and former staff of the Anglo-Australian Observatory for their work in building and operation of the AAOmega facility. This work used the CFHTLS data products, which is based on observations obtained with MegaPrime/MegaCam, a joint project of CFHT and CEA/DAPNIA, at the Canada-France-Hawaii Telescope (CFHT) which is operated by the National Research Council (NRC) of Canada, the Institut National des Sciences de l'Univers of the Centre National de la Recherche Scientifique (CNRS) of France, and the University of Hawaii. This work is based in part on data products produced at TERAPIX and the Canadian Astronomy Data Centre as part of the Canada-France-Hawaii Telescope Legacy Survey, a collaborative project of NRC and CNRS. CSS, PPJ and RS gratefully acknowledge support from the Indo-French Center for the Promotion of Advanced Research (Centre Franco-Indien pour la Promotion de la Recherche Avancée) under contract No. 3004-3.

REFERENCES

- Alexander D. M., et al. 2003, *AJ*, 126, 539
 Antonucci R., 1993, *ARA&A*, 31, 473
 Anderson J., et al. 2007, *AJ*, 133, 313
 Arnouts S., et al. 2005, *ApJL*, 619, 43
 Avni Y., Tananbaum H., 1986, *ApJ*, 305, 83
 Baldwin J. A., Phillips M. M., Terlevich R., 1981, *PASP*, 93, 5
 Barger A.J. et al. 2003, *AJ*, 126, 632
 Bechtold J., et al. 2003, *ApJ*, 588, 119
 Bondi M., et al. 2003, *A&A*, 403, 857
 Bondi M., et al. 2007, *A&A*, 463, 519
 Brand K., et al. 2006, *ApJ*, 641, 140
 Brandt W. N., Hasinger G., 2005, *ARA&A*, 43, 827
 Brusa M., et al. 2003, *A&A*, 409, 65
 Brusa M., et al. 2007, *ApJS*, 172, 353
 Caccianiga A., et al. 2008, *A&A*, 477, 735
 Caccianiga A., Severgnini P., Della Ceca R., Maccacaro T., Carrera F. J., Page M. J., 2007, *A&A*, 470, 557
 Cappelluti N., et al. 2009, *A&A*, 497, 635
 Cohen A.S., et al. 2003, *ApJ*, 591, 640
 Cocchia F. et al. 2007, *A&A*, 466, 31
 Comastri A., et al. 2002, *ApJ*, 571, 771
 Condon J. J., Cotton W. D., Greisen E. W., Yin Q. F., Perley R.A., Taylor G. B., Broderick J. J., 1998, *AJ*, 115, 1693
 Croom S. M., Smith R. J., Boyle B.J., Shanks T., Loaring N.S., Miller L., Lewis I. J., 2001, *MNRAS*, 322, 29
 Dye S., et al. 2006, *MNRAS*, 372, 1227
 Elvis M., Schreier E.J., Tonry J., Davis M., Huchra J.P., 1981, *ApJ*, 246, 20
 Fabbiano G., Kim D.W., Trinchieri G., 1992, *ApJS*, 80, 531
 Feruglio C., et al. 2008, *A&A*, 488, 417
 Fiore F., et al. 2003, *A&A*, 409, 79
 Fossati G., Maraschi L., Celotti A., Comastri A., Ghisellini G., 1998, *MNRAS*, 299, 433
 Garcet O., et al. 2007, *A&A*, 474, 473
 Gavignaud I. et al. 2006, *A&A*, 457, 79
 Georgantopoulos I., Georgakakis A., 2005, *MNRAS*, 358, 131
 Green P. J. et al. 2009, *ApJ*, 690, 644
 Griffiths R.E., Georgantopoulos I., Boyle B.J., Stewart G.C., Shanks T., della Ceca R., 1995, *MNRAS*, 275, 77
 Giacconi R. et al. 2002, *ApJS*, 139, 369
 Gibson R.R., Brandt W. N., Schneider D.P., 2008, *ApJ*, 685, 773
 Hasinger G., Burg R., Giacconi R., Schmidt M., Trumpler J., Zamorani G., 1998, *A&A*, 329, 482
 Hewett P.C., Foltz C. B., Chaffee F. H., 1995, *AJ*, 109, 1498
 Just D. W., Brandt W. N., Shemmer O., Steffen A. T., Schneider D. P., Chartas G., Garmire G. P., 2007, *ApJ*, 665, 1004
 Kauffmann et al. 2003, *MNRAS*, 346, 1055
 Kelly, B. C., Bechtold, J., Siemiginowska, A., Aldcroft, T., Sobolewska, M. 2007, *ApJ*, 657, 116
 Kewley L.J., Heisler C. A., Dopita M.A., Lumsden S., 2001, *ApJS*, 132, 37
 Krumpe M., et al. 2007, *ARA&A*, 466, 41
 La Franca, F., Franceschini, A., Cristiani, S., Vio, R. 1995, *A&A*, 299, 19
 Lawrence A., et al. 2007, *MNRAS*, 379, 1599
 Lehmann I., et al. 2001, *A&A*, 371, 833
 Le Fevre O., et al. 2004, *A&A*, 417, 839
 Lewis I. J., et al. 2002, *MNRAS*, 333, 279
 Lonsdale C. J., et al. 2003, *PASP*, 115, 897
 Luo B., et al. 2008, *ApJS*, 179, 19
 Maccacaro T. et al. 1982, *ApJ*, 253, 504
 Miszalski B., Shorridge K., Saunders W., Parker Q.A., Croom S. M. 2006, *MNRAS*, 371, 1537
 Oke J.B., Gunn J. E., 1983, *ApJ*, 266, 713
 Pickering T. E., Impey C.D., Foltz C. B., 1994, *AJ*, 108, 1542
 Pierre M., et al. 2004 *JCAP*, 09, 011
 Pierre M., et al. 2007, *MNRAS*, 382, 279
 Reimers D., Koehler T., Wisotzki L., 1996, *A&AS*, 115, 235
 Severgnini, P., Caccianiga, A., & Braitto, V. 2003, *A&A*, 467, 73
 Schmidt M., Green R. F., 1983, *ApJ*, 269, 352
 Schiminovich D., et al. 2005, *ApJL*, 619, 47
 Schneider D. P., et al. 2007, *AJ*, 134, 102
 Schultheis M., Robin A.C., Reyle C., McCracken H. J., Bertin E., Mellier Y., Le Fevre O., 2006, *A&A*, 447, 185
 Schwoppe A. D., et al. 2000, *Astron. Nachr.* 321, 1
 Sharp R., et al. 2006, in McLean I.S., Iye M., eds, *Proceed-*

ings of the SPIE, Vol. 6269, Ground-based and Airborne Instrumentation for Astronomy (astro-ph/0606137)
 Shen S., White, S.D.M., Mo J.H., Voges W., Kauffmann G., Tremonti C., Anderson S.F., 2006, MNRAS, 369, 1639
 Spoon H. W. W., Keane J. V., Tielens A. G. G. M., Lutz D., Moorwood A. F. M., 2001, A&A, 365, L353
 Stalin C.S., Srianand R., Petitjean P., 2009a *in preparation*
 Stalin C.S., Srianand R., Petitjean P., 2009b *in preparation*
 Steffen A.T., et al. 2006, AJ, 131, 2826
 Stern D., Djorgovski S. G., Perley R. A., de Carvalho, Reinaldo R., Wall J.V., 2000, AJ, 119, 1526
 Stocke J. T. et al. 1991, ApJS, 76, 813
 Strateva, I. V., Brandt, W. N., Schneider, D. P., Vanden Berk, D. G., 2005, AJ, 130, 387
 Szokoly G. P., et al. 2004, ApJS, 155, 271
 Tasse C., Rottgering H.J.A., Best P.N., Cohen A.S., Pierre M., Wilman R., 2007, A&A, 471, 1105
 Tajer M., et al. 2007, A&A, 467, 73
 Trump J. R., et al. 2009, ApJ, 696, 1195
 Ueda Y., Akiyama M., Ohta K., Miyaji T., 2003, ApJ, 598, 886
 Ueda Y. et al. 2008, ApJS, 179, 124
 Vignali, C., Brandt, W. N., Schneider, D. P., Garmire, G. P., 2003, AJ, 125, 418
 Wang J.X., et al. 2004, AJ, 127, 213
 Wilkes B.J., Elvis, M., 1987, ApJ, 323, 243
 Wilkes B. J., Tananbaum H., Worrall D. M., Avni Y., Oey M. S., Flanagan J., 1994, ApJS, 92, 53
 Worrall D.M., Tananbaum H., Giommi P., Zamorani G., 1987, ApJ, 313, 596
 Worrall D.M., Birkinshaw M., 2006 (astro-ph/0410297)
 Yang Y., Mushotzky R.F., Steffen A.T., Barger A. J., Cowie L. L., 2004, AJ, 128, 1501
 Yuan W., Brinkmann W., Siebert J., Voges W., 1998, A&A, 330, 108
 Yuan F., Narayan R., 2004, ApJ, 612, 724
 Zamorani G., et al. 1981, ApJ, 245, 357

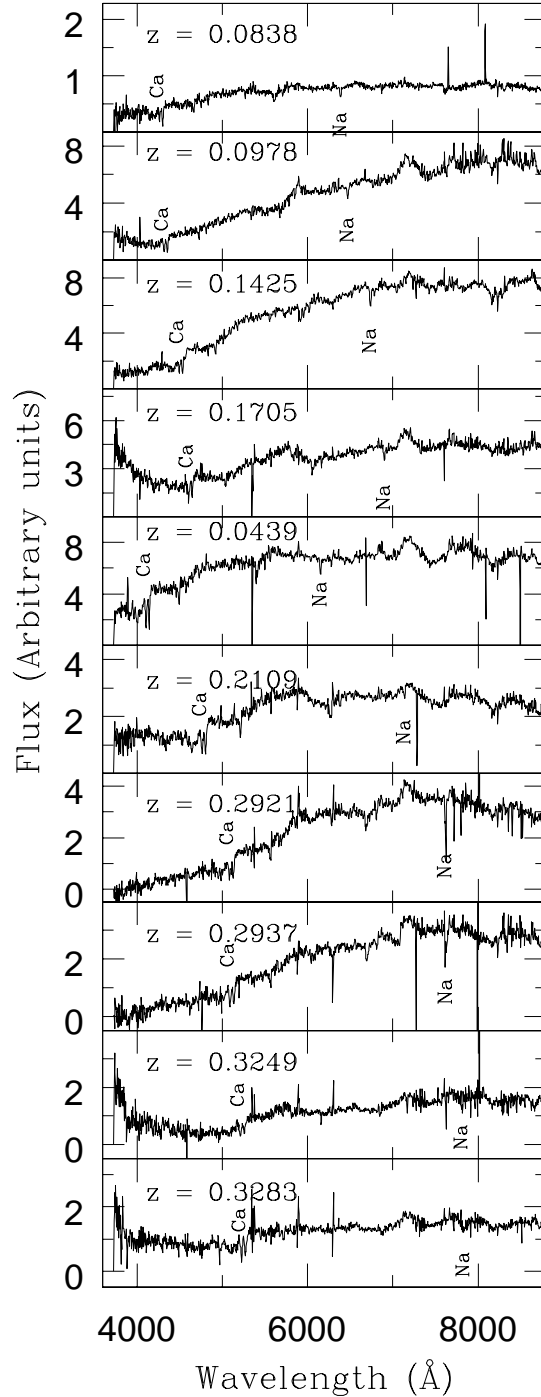


Figure 6. Examples of optical spectra of absorption-line galaxies. Redshifts are indicated on each panels. The Na absorption line is marked and the region where Ca H & K lines are found is indicated as Ca.

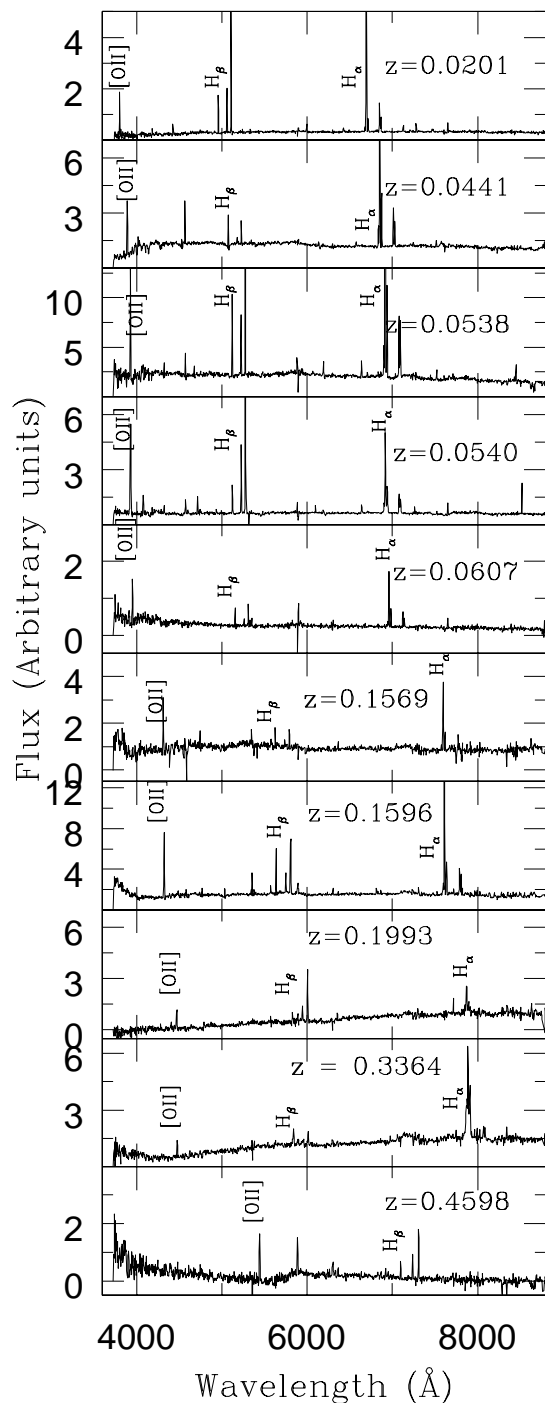


Figure 7. Examples of optical spectra of emission-line galaxies. The redshift of each galaxy is given in the corresponding panel. The prominent emission lines are marked

and

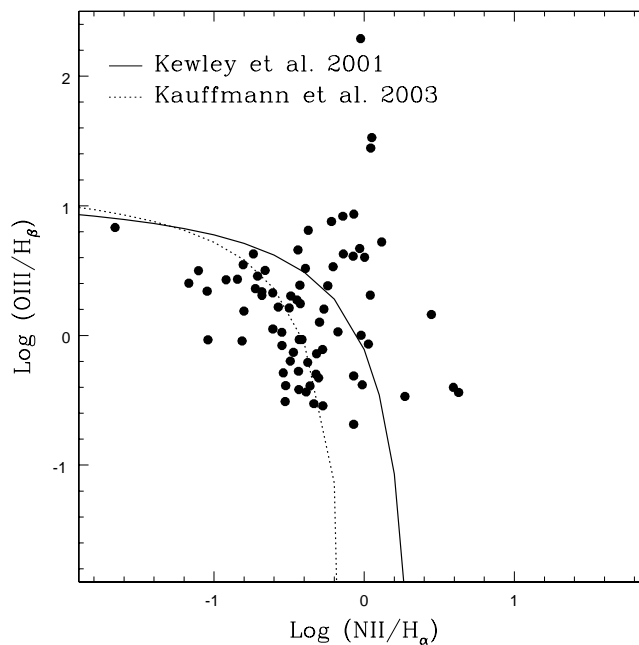


Figure 8. The Baldwin-Phillips-Terlevich (BPT) diagnostic diagram for the emission line objects with [OIII], H β , [NII] and H α detected in their optical spectra. Objects above and below the lines are powered by AGN and starbursts respectively. The solid line is that of Kewley et al. (2001) and the dotted line is that of Kauffmann et al. (2003).

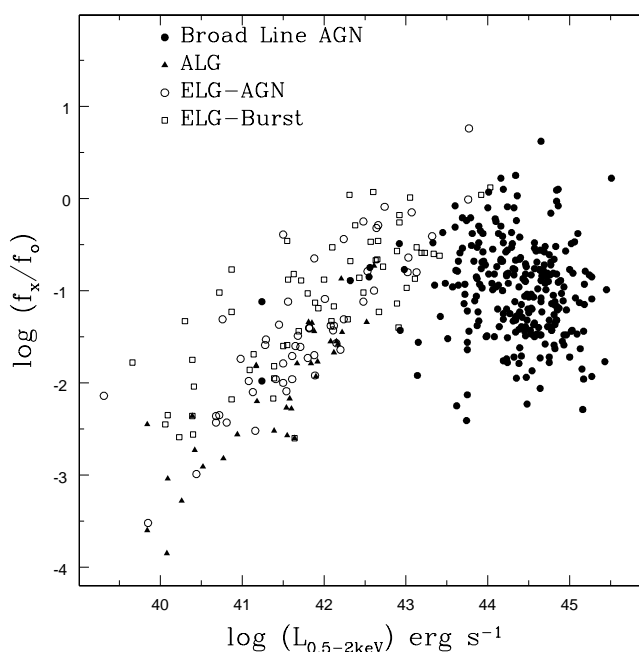


Figure 9. X-ray to optical flux ratio (f_x/f_o) plotted against the intrinsic X-ray luminosity $L_{0.5-2keV}$

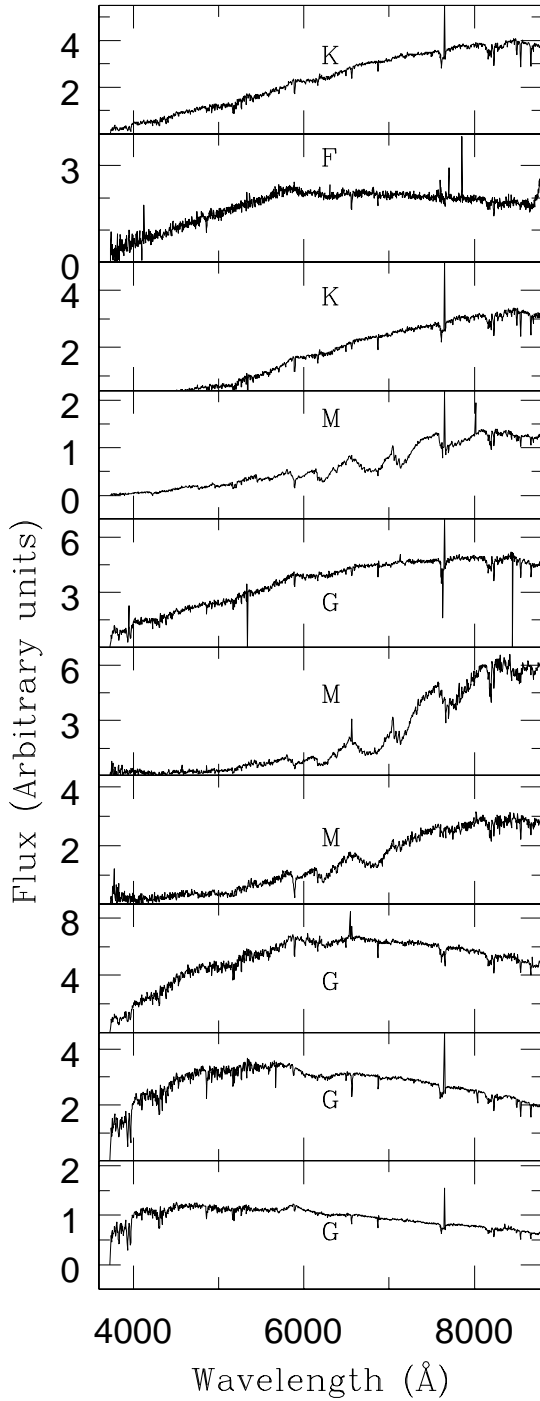


Figure 10. Examples of the optical spectra of stars. Their spectral types are given on each panel.

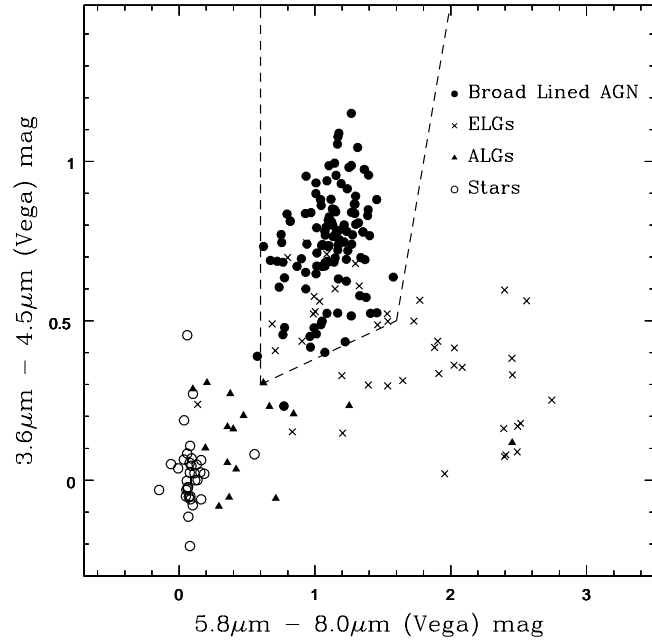


Figure 11. Positions of the various kinds of XMM sources in the IR colour-colour diagram. Here filled circles are broad-line AGNs, crosses are emission-line galaxies, filled diamonds are absorption-line galaxies and open circles are stars. The dotted line is the empirical region of Stern et al. (2005) used to separate AGN from stars and galaxies.

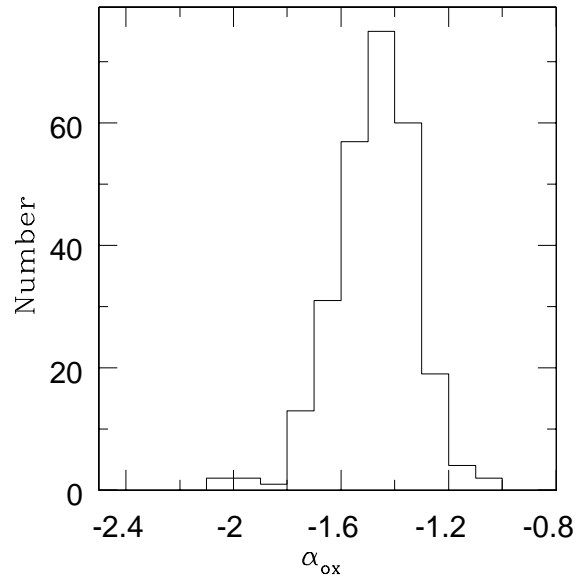


Figure 12. Distribution of α_{ox} for the spectroscopically identified broad-line AGNs in our sample of XMM sources.

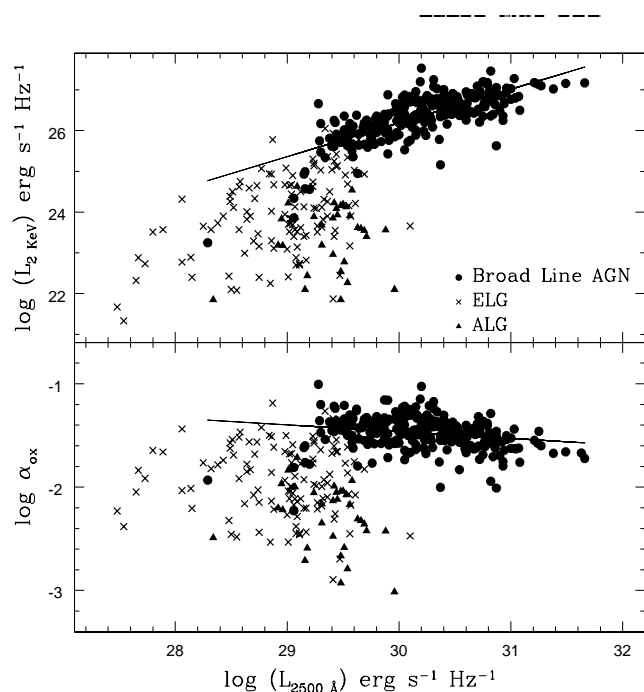


Figure 13. *Top panel:* Plot of the rest frame monochromatic luminosity at 2 keV versus the rest frame monochromatic luminosity at 2500 Å. *Bottom panel:* plot of α_{ox} against the rest frame monochromatic luminosity at 2500 Å. Symbols have the same meaning as in Fig. 4. The solid line is the linear least squares fit to only the broad-line AGNs

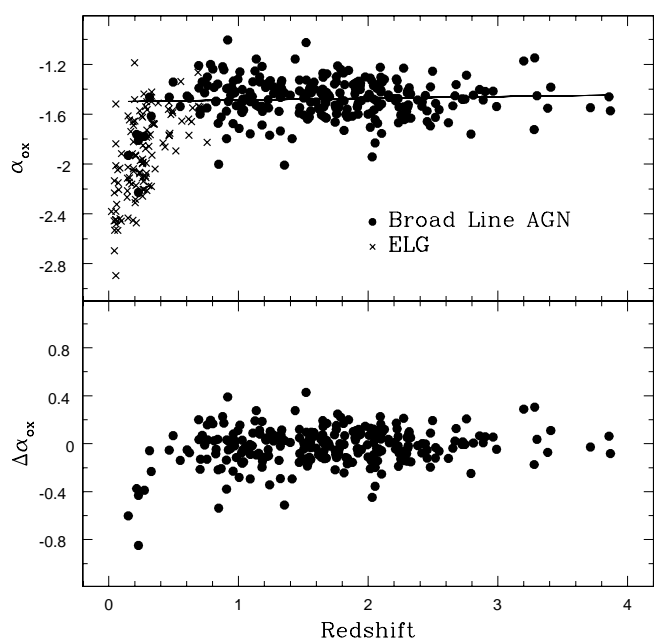


Figure 14. *Top panel:* α_{ox} versus redshift for broad-line AGNs and ELGs (as some of the ELGs are powered by AGN). The solid line is the linear least squares fit to only the broad-line AGNs. *Bottom panel:* Residual in α_{ox} plotted against redshift for only broad line AGNs. Symbols are the same as in Fig. 4.